Journal Pre-proof

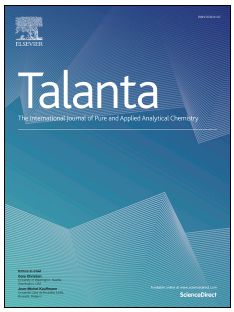

Nanoparticle core size and spacer coating thickness dependence on metal-enhanced luminescence in optical oxygen sensors

Wenwen Yin, Jiajie Sui, Guozhong Cao, Dana Dabiri

PII: S0039-9140(22)00486-6

DOI: https://doi.org/10.1016/j.talanta.2022.123690

Reference: TAL 123690

To appear in: *Talanta*

Received Date: 12 April 2022

Revised Date: 11 June 2022

Accepted Date: 13 June 2022

Please cite this article as: W. Yin, J. Sui, G. Cao, D. Dabiri, Nanoparticle core size and spacer coating thickness dependence on metal-enhanced luminescence in optical oxygen sensors, *Talanta* (2022), doi: https://doi.org/10.1016/j.talanta.2022.123690.

CRediT author statement

Wenwen Yin: Conceptualization, Investigation, Methodology, Software, Validation, Visualization, Writing - Original Draft

Jiajie Sui: Investigation

Guozhong Cao: Conceptualization, Methodology, Supervision, Project Administration.

Dana Dabiri: Conceptualization, Methodology, Writing- Reviewing and Editing, Supervision, Funding Acquisition, Project Administration.

Nanoparticle core size and spacer coating thickness dependence on metal-enhanced luminescence in optical oxygen sensors

Wenwen Yin[a#], Jiajie Sui[b$], Guozhong Cao[b], Dana Dabiri[a*]

[a] Department of Aeronautics & Astronautics, University of Washington, Seattle WA 98195-2120, USA.

[b] Department of Materials and Engineering, University of Washington, Seattle WA 98195-2120, USA.

Present Addresses:
[#] Sun Yat-sen University, 2 Daxue road, Zhuhai, China, 519000
[$] University of Wisconsin-Madision, 1500 Engineering Drive, Madison, WI 53715

Corresponding Author
*E-mail: dabiri@uw.edu

ABSTRACT: Metal-enhanced luminescence (MEL) originated from near field interactions of luminescence with the surface plasmon resonance (SPR) of nearby metallic nanoparticles (NPs) is an effective strategy to increase luminescence detection sensitivity in oxygen sensors. Once the excitation light induces SPR, the generated enhanced local electromagnetic filed will result in an enhanced excitation efficiency and an increased radiative decay rates of luminescence in close proximity. Meanwhile, the nonradioactive energy transfer from the dyes to the metal NPs, leading to emission quenching, can also be affected by their separation. The extent of the intensity enhancement depends critically on the particle size, shape and the separation distance between the dye and the metal surface. Here, we prepared core-shell Ag@SiO_2 with different core sizes (35 nm, 58 nm and 95 nm) and shell thickness (5-25 nm) to investigate the size and separation dependence on the emission enhancement in oxygen sensors at 0-21% oxygen concentration. Intensity enhancement factors of 4-9 were observed with a silver core size of 95 nm and silica shell thickness of 5 nm at 0-21% O_2. In addition, the intensity enhancement factor increases with increasing core size and decreasing shell thickness in the Ag@SiO_2-based oxygen sensors. Using Ag@SiO_2 NPs result in brighter emission throughout the 0-21% oxygen concentration. Our fundamental understanding of MEP in the oxygen sensors provides us the opportunity to design and control efficient luminescence enhancement in oxygen and other sensors. .

Keywords: Metal enhanced luminescence; Surface plasmon resonance; Separation distance; Emission quenching; Emission enhancement.

Graphical abstract

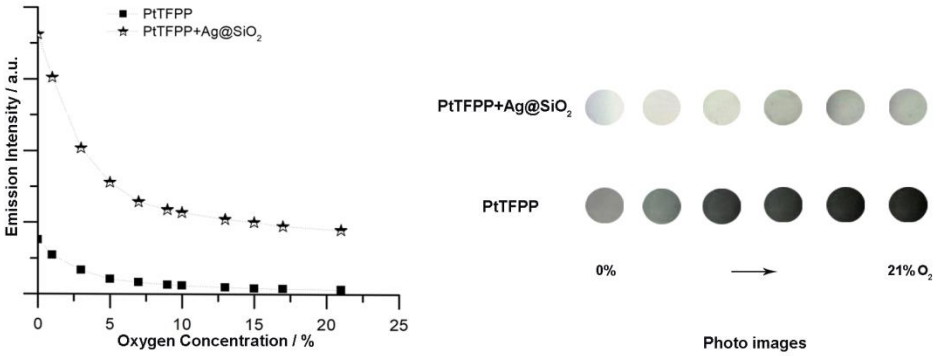

In the MEL-based oxygen sensors, the emission intensity can be greatly enhanced. The enhanced factor is highly dependent on the separation between the dyes and the noble metal surface and the spectral overlap between the LSPR of noble metal and the excitation spectra of dyes. In this paper, we elaborate on the dependence of the sensitivity and emission intensity on the separation distance from the metal surface by varying the silica shell thickness (5-25 nm), and the Ag NP size (35 nm, 58 nm and 95 nm) in the optical oxygen sensors under varied oxygen pressure. Our results demonstrate that the intensity increases with increasing core size and decreasing shell thickness. The intensity of the 95 nm Ag@5 nm SiO_2-PtTFPP based oxygen sensors is the highest among these samples, resulting in 4-9 fold brighter intensity than that of PtTFPP-based oxygen sensors at 0-21% O_2.

1. Introduction

Metal enhanced luminescence (MEL)-based oxygen sensors that combine noble metal nanoparticles (NPs) with dyes is a novel and sensitive detection technique for oxygen concentrations [1-3]. In the luminescence-based sensors, once the luminescence dyes are excited, they will emit fluoresce or phosphorescence. Combined noble metal NPs in the sensors, once the excitation light induces surface plasmon resonance (SPR), the generated enhanced local electromagnetic filed will result in an enhanced excitation efficiency and an increased radiative decay rates of fluoresce [4] or phosphorescence [5,6]. Take the fluorophore for instance, as shown in fig.1, the fluorophore can also return to the ground state by non-radiative decay with a rate (k_{nr}) or due to some other quenching process (k_q). Both the non-radiative decay and some other quenching processes compete with the emission of a photon (Γ), leading to the low quantum yield (Q_0). In the presence of noble metal NPs, there will be an enhanced absorption and emission (Γ_m) under the effect of noble metal NPs, contributing to the increment of quantum yield (Q_m) [7]. Noble metal NPs exhibit localized surface plasmon resonance (LSPR) due to the interaction between incident light and surface electrons in the metal conduction band. The LSPR depended on the particle material, shape and size can lead to a large enhancement in the absorption and scattering of light [8-10]. When the luminescent dyes are placed in the vicinity of noble metal NPs, both the excitation rate and emission rate will be greatly increased under the local field enhancement effect [11]. In the MEL-based oxygen sensors, the emission intensity can be greatly enhanced, which is highly dependent on the separation between the dyes and the noble metal surface and the spectral overlap between the LSPR of noble metal and the excitation spectra of dyes [12]. Understanding and controlling these effects is thus essential for taking advantage of the plasmon-exciton interaction in designing and developing MEL-based oxygen sensors.

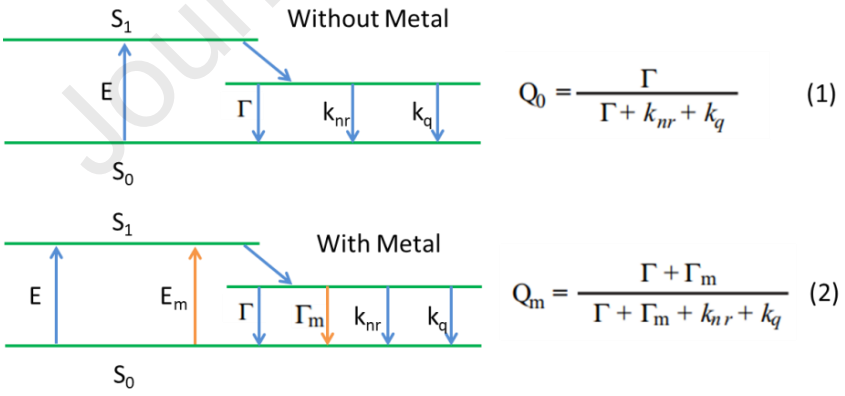

Fig.1. Modified Jablonski diagram for metal-enhanced fluorescence: Q_0 and Q_m are quantum yields of fluorophore without and with noble metal.

It has been reported that the emission of dyes will be either quenched [13] or enhanced [14] by the electromagnetic field generated at the surface of metal NPs upon resonant excitation. In general, there is strong quenching with the separation distance of the dye-metal less than 5 nm; maximum enhancement factors occur at 8 nm, which then decrease rapidly with further increasing separation distance [15, 16]. The MEL is related to both the increased excitation rate under the local field enhancement effect and the electromagnetic coupling of the dye with the

metal NP [17]. It will allow the excitation energy to non-radioactively partially transfer from the dyes to the metal NPs and also transmit the energy of the dye as radiation to the far field, which leads to two opposite results. On one hand, quenching of the dye emission occurs up to 5 nm from the metal surface; On the other hand, the electrical field enhancement decays exponentially from the metal NP surface outwards [18,19]. Consequently, precise control of the separation distance between the dyes and noble metal surfaces is vital in the design and performance of design and performance of MEL-based oxygen sensors.

To control the strong separation distance dependence on metal/dye interactions, a variety of spacer materials, including silica [20, 21], DNA [22, 23] and polymers [24, 25] have been used. The disadvantage of using DNA and polymers as spacers is that they are so flexible that it is difficult to completely control the metal/dye separation distance, even failing to prevent dye-metal contact, leading to emission quenching [19]. On the contrary, the rigid silica spacers can be easier to control with nanometer precision to effectively avoid dye-metal contact. Besides, the silica layers can protect the metal core from chemical reactivity with the analytes. The size and shape of the metal core can also be optimized for specific applications [26]. There are many reports in the literatures that have detail recipes of coating silica spacers on noble metal NPs, from 3 to 90 nm, lead to large emission enhancements in MEL [20, 21, 27]. To establish the relationship between emission enhancement and metal/dye separation distance in the optical oxygen sensors, we prepared hybrid metallic nanostructures consisting of a silver core and a silica shell with precisely controlled thickness. The rigid surface of silica shell on the Ag NPs can effectively prevent quenching of the fluorescence dyes by the metal through maintaining a fixed metal/dye separation [20]. We elaborate on the dependence of the sensitivity and emission intensity on the separation distance from the metal surface by varying the silica shell thickness (5-25 nm), and the Ag NP size (35 nm, 58 nm and 95 nm) in the optical oxygen sensors under varied oxygen pressure. Our results demonstrate that the intensity increases with increasing core size and decreasing shell thickness. The intensity of the 95 nm Ag@5 nm SiO_2-PtTFPP based oxygen sensors is the highest among these samples, resulting in 4-9 fold brighter intensity than that of PtTFPP-based oxygen sensors at 0-21% O_2. The Ag@SiO_2 exhibits brighter emission, throughout the range of the oxygen concentration, which is great progress in applications of oxygen sensors and helpful in other gas sensors.

2. Experimental section

2.1. Sample preparation

2.1.1. Synthesis of Ag NPs

(1) Au seeds preparation: In a typical synthesis for ~3 nm Au seeds, 5 ml of PVP (5 wt% in H_2O) and 10 µl of $HAuClO_4$ (0.25 M) were dissolved in 5 ml H_2O [28]. After that, 0.6 ml of $NaBH_4$ (0.1 M) was injected under vigorous stirring. The as-prepared Au nanoparticles were then aged for 6 h, allowing complete decomposition of $NaBH_4$ before the subsequent seeded growth procedure.

(2) Ag NPs: In a typical synthesis of 40 nm Ag quasi-NPs, 2 ml PVP (5 wt% in H_2O), 2 ml acetonitrile, and 100 µl ascorbic acid (0.1 M) were added in 2 ml H_2O, which was thermostatized at 10℃. Then, 150 µl $AgNO_3$ (0.1 M) was added, followed by quick injection of 10 µl seed solution. The Ag quasi-NPs were finally collected by centrifugation and repetitively washed with H_2O. To synthesize Ag quasi-NPs of other sizes, the reaction temperature was adjusted for favorable reaction kinetics, in addition to a change in the volume of the seed solution.

2.1.2. Synthesis of $Ag@SiO_2$

4 ml 16-mercaptohexadecanoic acid (MHA) (1 mM) was slowly added to the ml Ag quasi-NPs solution, and the resultant solution was then mixed with 76 ml ethanol [29]. After that, 4 ml Diethylamine and 20-160 µl tetraethyl orthosilicate (TEOS) were added in sequence while stirring and the reaction was allowed to proceed for 90 min. The volume of TEOS is varied for different thicknesses of SiO_2 (20 ul: 5 nm; 50 ul: 10 nm; 100 ul: 15nm; 160 ul: 25 nm). This afforded a colloid of $Ag@SiO_2$ NPs after centrifugation and dispersion in EtOH.

2.2. Fabrication of $Ag@SiO_2$ based oxygen sensors

Octyl-triEOS/TEOS composite sol-gel was used as the matrix material in the PSP and prepared by mixing Octyl-triEOS (0.20 ml) and TEOS (4.00 ml) to form a precursor solution according to Chu's method [1]. EtOH (1.25 ml) and HCl (0.1 M, 0.40 ml) were then added to the sol-gel solution to catalyze the ORMOSIL reaction. The resulting solution was stirred magnetically for 1 h at room temperature. Then 0.10 ml Triton-X-100 was added to improve the homogeneity of the silica sol. 20 mg $Ag@SiO_2$ was added to 0.50 ml PtTFPP/EtOH (0.2 mg/ml) solution and stirred for 12 h. Then 0.50 ml composite sol-gel solution was added to the dye solution. Finally, the solution was capped and stirred magnetically for another 12 h. Before the response test to oxygen concentration, 200 ul sol-gel solution was dropped onto a glass slide (2*2 cm^2) and left to stabilize under ambient conditions for 24 h.

3. Results and discussion

3.1. Results

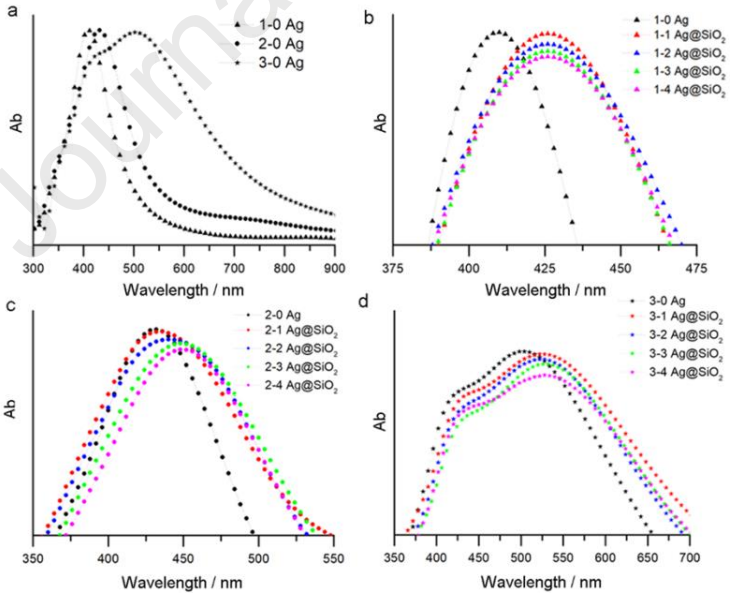

Fig.2. UV-Vis spectra of **a** Ag NPs and **b-d** $Ag@SiO_2$ NPs with different core size and different thickness.

In a typical synthesis, a seeded growth method is employed to prepare monodisperse Ag NPs with different size range of 19-140 nm in a large quantity. In this work, we use the seeded growth method to prepare three sizes of Ag NPs (1-0: 35 nm; 2-0: 58 nm; 3-0: 95 nm) using the

recipes from Liu *et al.* (2013) [28]. UV-vis spectroscopy of Ag quasi-NPs (**Fig.2a**) in water was investigated to reveal their optical properties. It clearly demonstrates that the particle size plays a critical role in the optical properties of Ag NPs. As the size of Ag NPs increases, the absorbance peak shifts to longer wavelength, which are centered at 410, 430, 504 nm for Ag NPs of 35, 58 and 95 nm, respectively. When the particle size is above 80 nm, a shoulder appears at 419 nm, corresponding to a quadrupolar plasmon resonance, which becomes well resolved if the particle size becomes even larger. All these spectral features are in good agreement with those simulated by the Mie theory [28]. The Ag NPs obtained were then transferred to ethanol with the aid of 16-mercaptohexadecanoic acid (MHA) and then coated with a silica layer by a sol-gel reaction of tetraethyl orthosilicate (TEOS) [29]. Uniform silica coating over silver NPs was achieved by Stöber condensation reaction and the shell thickness was varied by controlling the amount of TEOS [30]. As shown in the **Fig.2b-d**, three sizes of Ag NPs coated with different amount of TEOS (20 ul; 50 ul; 100 ul; 160 ul) were prepared. The UV-vis spectra indicate that the plasmonic peaks of Ag@SiO_2 red shift and are broader than that of bare Ag NPs **(Table S1)**. With increasing amounts of TEOS (from red dot to pink red in **Fig.2b-d**), the plasmonic peaks of Ag@SiO_2 also red shifts and become broad, which are attributed to the thicker silica on the surface of Ag NPs [30].

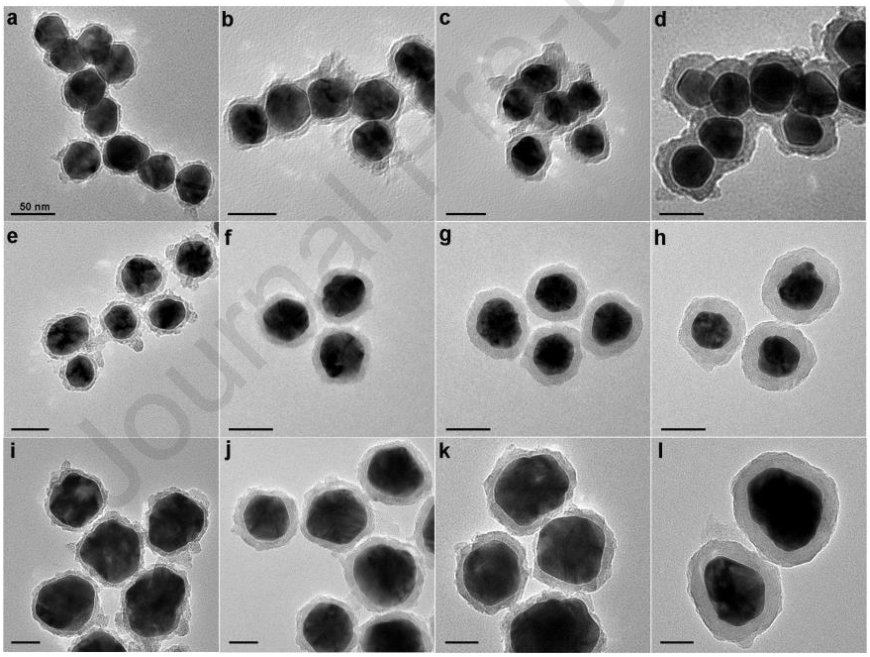

Fig.3. TEM images of Ag@SiO_2 with different core sizes and thicknesses. The top, middle and bottom rows are 35(1-0), 58(2-0) and 95(3-0) nm Ag NPs, respectively, and the columns from left to right are the Ag@SiO_2 thickness at 5, 10, 15, 25 nm, respectively. Specifically, (**a**) 1-1: 35 nm Ag@5 nm SiO_2, (**b**) 1-2: 35 nm Ag@10 nm SiO_2, (**c**)1-3: 35 nm Ag@15 nm SiO_2, (**d**)1-4: 35 nm Ag@25 nm SiO_2; (**e**) 2-1:58 nm Ag@5 nm SiO_2, (**f**)2-2: 58 nm Ag@10 nm SiO_2, (**g**)2-3: 58 nm Ag@15 nm SiO_2, (**h**)2-4: 58 nm Ag@25 nm SiO_2;(**i**)3-1: 95 nm Ag@5 nm SiO_2, (**j**)3-2: 95 nm Ag@10 nm SiO_2, (**k**)3-3: 95 nm Ag@15 nm SiO_2, (**l**)3-4: 95 nm Ag@25 nm SiO_2. All scale bars are 50 nm.

The size of the Ag core and silica shell thickness in each case was further tested using

transmission electron microscopic (TEM) analysis. Three sizes of silver NPs in this paper with diameters of 35 nm, 58 nm and 95 nm were prepared using the recipe reported by Liu *et al.* [28]. The TEM image in **Fig.3** reveals that the silica layer thickness of Ag@SiO_2 from left to right (**Fig.3 a-d, e-h, i-l**) is 5 nm, 10 nm, 15 nm and 25 nm, respectively. It was found that the Ag@SiO_2 with 35 nm core size aggregated more than that those with 58 nm and 95 nm core size, which might be due to the small size Ag NPs being easier to aggregate in the solution. Comparing the Ag@SiO_2 from left to right, it can be seen that the SiO_2 coating for Ag@5 nm SiO_2 is less uniform and rough; while for 10-25 nm SiO_2 on Ag surface, the silica layer is more uniform. It is understandable that thicker coating procedure is easier to control than thinner coating for preparing Ag@SiO_2 NPs. By adjusting the volume of TEOS, Ag@SiO_2 NPs with different thicknesses were prepared.

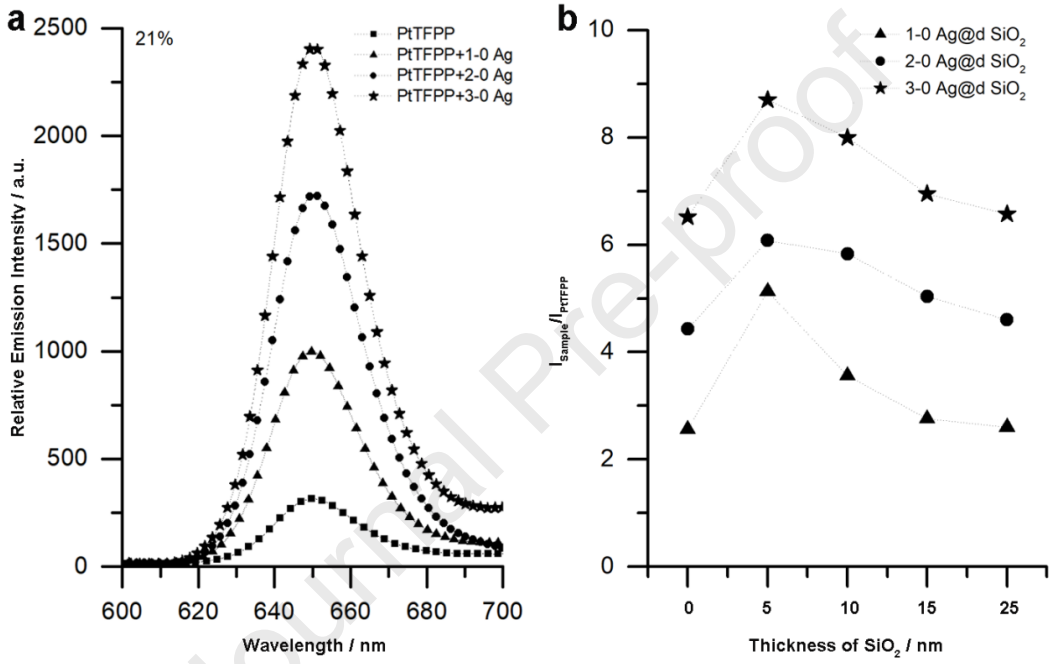

Fig.4 (a) Emission spectra of PtTFPP-based oxygen sensors mixed with 5% wt. Ag NPs at 21% O_2; (**b)**Dependence of the intensity enhancement factor of PtTFPP-NPs based oxygen sensors compared with PtTFPP-based oxygen sensor (I_{sample}/I_{PtTFPP}) on the silica shell thickness at 21% O_2.

MEL is highly dependent on the size of NPs and separation distance between NPs and dyes. To further investigate the effect in the optical oxygen sensors, emission spectra of PtTFPP-based oxygen sensors mixed with different sizes of Ag NPs at 21% O_2 were tested. The emission spectrum of PtTFPP-based oxygen sensors was also recorded as a baseline reference for comparison. The intensity of PtTFPP-based oxygen sensor in **Fig.4a** is just about 300 at 21% O_2, while, the intensity of PtTFPP-1-0 Ag based oxygen sensor (35 nm Ag NPs, black triangle) is about 1000. The intensity of PtTFPP-based oxygen sensors mixed with 58 nm Ag NPs (black dot) and 95 nm Ag NPs (black star) are as high as 1700 and 2400, respectively. It can be clearly seen that the intensity of PtTFPP-Ag NPs based oxygen sensors is highly dependent on the size of Ag NPs. Among these three sizes of Ag NPs, the PtTFPP-based oxygen sensor with 95 nm Ag NPs has the strongest emission. Then the intensity of PtTFPP-based oxygen sensors with different thicknesses of SiO_2 on the Ag NPs was also compared. In order to have a clear insight into the dependence of

the luminescence enhancement factor on the size of the Ag NPs and their silica coating thickness, the intensity of PtTFPP-Ag@SiO_2 based oxygen sensor compared with that of PtTFPP based oxygen (I_{sample}/I_{PtTFPP}) at 21% O_2 vs. silica thickness was plotted in **Fig.4b**. The enhancement factor of the PtTFPP-Ag based oxygen sensors increases from 2.6 to 4.4 and 6.5 for the Ag NP size, increasing from 40 nm to 58 nm and 95 nm, respectively. These results further demonstrate that the intensity enhancement factor of PtTFPP-based oxygen sensors increase with the size of Ag NPs; the 95 nm Ag NPs, is largest among these three Ag NP sizes synthesized in our work. The emission amplification of PtTFPP-Ag@SiO_2 based oxygen sensors for 40 nm Ag is 5.1, 3.6, 2.8 and 2.60 for silica shell thickness increasing from 5 nm, 10 nm to 15 nm and 25 nm, respectively. For 58 nm Ag, the emission enhanced factor is 6.11, 5.8, 5 and 4.60 for silica shell thickness increasing from 5 nm, 10 nm to 15 nm and 25 nm, respectively. For 95 nm Ag, the intensity amplification is 8.70, 8.00, 6.95 and 6.66 for silica shell thickness increasing from 5 nm, 10 nm to 15 nm and 25 nm, respectively. Clearly, the intensity enhancement for Ag@SiO_2 NPs with the same shell thickness increases with the increment of the Ag core size from 35 nm to 95 nm, which can be ascribed to the continuous increased scattering cross section of the sliver core. Based on the theoretical calculations in previous Ag@SiO_2reports about MEL systems, the enhanced electric field plays a dominant role in the overall emission enhancement of dyes. With increasing silver core size, the electric field extends further out from the metal and the intensity decreases with the separation distance to the metal surface. When the silver core size is larger than 80 nm, the electric field tends to exhibit a quadrupolar resonance. Their calculation results indicate that a maximum enhancement can be achieved around an 80 nm Ag NP core size [27]. In addition, with increasing shell thickness, the electric field enhancement decreases and the maximum enhancement was generally obtained around 5 nm, which is almost the same as that reported for MEL [31]. Among the Ag@SiO_2 NPs we prepared, the 95 nm Ag@5 nm SiO_2 NPs exhibited the largest intensity enhancement, which is identical to the results in the previous MEL reports [27, 31].These results suggest that the optimal separation distance between dyes and Ag NP surfaces and core size are critical to obtain maximum emission intensity in optical oxygen sensors.

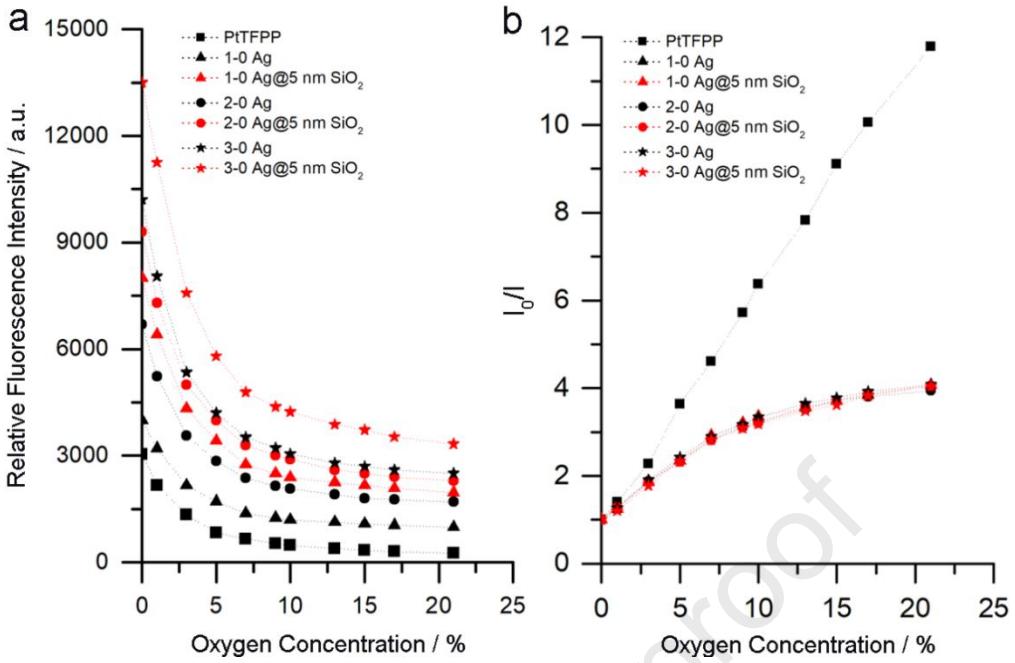

Fig.5(a) Emission intensity and **(b)** Stern-Volmer plot of PtTFPP-NPs based oxygen sensor under different concentration of oxygen (0-21% O_2).

To have a further insight into the effect of core size and thickness of silica on response of PtTFPP based oxygen sensors, the emission intensity and Stern-Volmer plot of PtTFPP-based oxygen sensors mixed with Ag and Ag@5 nm SiO_2 were tested and plotted in **Fig.5**. It can be seen from the intensity in **Fig.5a** that as the oxygen concentration increases from 0% to 21%, the intensity of the PtTFPP-based oxygen sensor (black squares) decreases from 3600 to 300 (12 fold). For the PtTFPP-35 nm Ag-based oxygen sensor (black triangle) in **Fig.5a**, at 0-21% O_2, the intensity greatly decreases, from 4500 to 1000 (4.5 fold). The intensity of PtTFPP-35 nm Ag@5 nm SiO_2 (red triangle) decreases from 8000 to 2000 (4.0 fold). The emission intensities of PtTFPP-58 nm Ag (black diamond) and PtTFPP-58 nm Ag@ 5 nm SiO_2 (red diamond) decrease from 7000 to 1700 (4.1-fold) and 9500 to 2500 (3.8-fold) with the oxygen concentration increasing from 0% to 21%, respectively. For PtTFPP-95 nm Ag (black star) and PtTFPP-95 nm Ag@5 nm SiO_2 (red star), as the concentration increases from 0% to 21%, the intensity decreases from 10400 to 2500 (4.06-fold) and 13500 to 3300 (4.06-fold), respectively. Among these three sizes of Ag NPs, the emission intensities of PtTFPP-95 nm Ag based oxygen sensors and PtTFPP-95 nm Ag@ 5 nm SiO_2 are highest throughout the 0-21% O_2 range. Compared with PtTFPP-based oxygen sensors, the intensities of PtTFPP-based oxygen sensors with 35 nm Ag, 35 nm Ag@5 nm SiO_2, 58 nm Ag, 58 nmAg@5 nm SiO_2, 95 nm Ag and 95 nm Ag@ 5 nm SiO_2 are 2.92, 5.85, 4.86, 6.83, 7.44 and 9.90 times larger, respectively, at the same oxygen concentrations. In addition, the 5 nm SiO_2 spacer to the 35 nm, 58 nm, and 95 nm Ag NPs resulted in a factor of 2, 1.4, and 1.33 times intensity increase compared with their respective Ag NPs without SiO_2 spacers. The Stern-Volmer plots of these data, shown in **Fig.5b,** show that these curves collapse regardless of the base Ag core size, or whether they have SiO_2 spacers. Our results also clearly show that, the largest core size NP, 95 nm Ag@ 5nm SiO_2, is suitable in the case that requires the brightest emission.

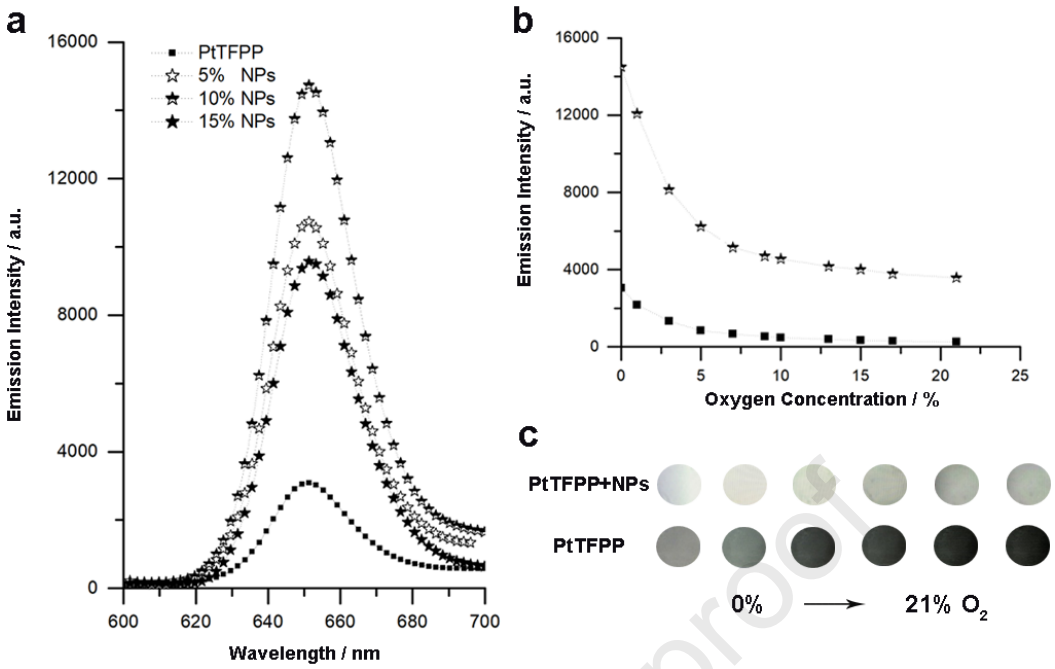

Fig.6 (a) Emission intensities of PtTFPP-95 nm Ag@5 nm SiO_2 oxygen sensors with different volumes of NPs at 0% O_2; **(b)** Emission intensity and **(c)** images of oxygen sensor under different concentration of oxygen.

In order to optimize the performance of Pt-NPs based oxygen sensors, we further investigate the dependence of emission intensity on the amount of NPs (95 nmAg@5 nmSiO_2). As shown in **Fig.6a**, the intensity of Pt-based oxygen sensors at 0.0% O_2 is about 3000. As the amount of NPs increases from 5% wt to 10% wt, the peak intensity increases from 11500 to 15000. As the number of NPs further increases to 15% wt, however, the peak intensity decreases to 9500. These data indicate that the intensity of PtTFPP-NPs based oxygen sensors is highly dependent on the number of NPs. In such systems, there are resonance energy transfers between dye molecules (homo RET), which involve self-quenching and non-radiative energy transfer (NRET) to the NPs [32]. If the PtTFPP molecules are too close to each other, self-quenching will occur. In addition, if the PtTFPP molecules are too close to the NPs, there will be NRET to the NPs. Both the self-quenching (RET) and NRET will lead to diminishing emission from the dyes. Only when these separation distances between the NPs are optimized can these losses be eliminated so that the phosphorescence emission, under the effect of the electromagnetic field of the NPs, be greatly enhanced. In cases where the volume of NPs is less than 10% wt, the number of NPs is not enough to accomplish this: the dyes are surrounded by more dye and less NPs, leading to more self-quenching and less MEL. At 10% wt NPs, the dyes are mostly surrounded by NPs, the MEL is strongest and thus the intensity is the brightest. When the amount of NPs is further increased to 15% wt, the NRET is dominated by the NPs, resulting in the decrease of phosphorescence intensity. Therefore, 10% wt. NPs is the optimal amount for the PtTFPP-Ag@SiO_2 based oxygen sensors. The emission intensity of the optimal PtTFPP-Ag@SiO_2-based oxygen sensor under different concentration of oxygen was also tested, the results of which are shown in **Fig.6b**. It can be clearly seen that the emission intensity of the PtTFPP-NPs based oxygen sensor with 10% wt NPs (star) is 4-fold higher than that of Pt-based

oxygen sensor (square) throughout the 0-21% O_2 concentration range, which is further confirmed by the brighter emission images of the PtTFPP-NPs based oxygen sensor versus the Pt-based oxygen sensor shown in **Fig.6c**.

3.2. Discussion

The LSPR that arises due to collective oscillation of electrons of the noble metal NPs can have either quenching [13] or enhancement [14] effects on the luminescence depending on the separation distance of the dyes from the metal surface and the relative position of the LSPR wavelength from the excitation wavelength of the dyes. This is applicable in MEL-based oxygen sensors, since the dye's intensity can also be enhanced or diminished by their surrounding metal NPs, as determined by the metal/dye separation distance and spectra overlap. Plasmon enhancement of dyes could be attributed to two opposing phenomena: an increased excitation rate induced by local field enhancement (LFE) and radiative decay rate by surface plasmon-coupled emission from coupling of the emission with the Ag NPs LSPR wavelength, resulting in emission enhancement, and the non-radiative energy transfer (NRET) from the dyes to the Ag NPs, resulting in emission quenching. The LFE effect drops off exponentially from the surface, while NRET process dominates at the surface and drops off with an inverse fourth power of localized electric field [33]. There is equilibrium between the LFE and NRET phenomena that affects the extent of emission enhancement. The LFE effect achieves its enhancement by increasing the excitation rate in the vicinity of dyes, which is dependent on many parameters including the dielectric permittivity of the metal, the nanoparticle NP size and the intrinsic quantum yield of dyes, especially the separation distance and excitation wavelength [16, 17]. These effects arise from variation of the radiative and non-radiative processes of luminescence via near-field interaction between dyes and metal NPs. These effects also result in either facilitating radiation to the far field or the energy transfer process of dyes to the metal surface. The NRET process between dyes and metal NPs can also enhance non-radiative decay rate and reduce the quantum yield of dyes, resulting in the reduced luminescence intensity. NRET depends mainly on separation distance between dyes and metal NPs and is independent of the excitation wavelength. Therefore, when dyes are in very close proximity of Ag NPs surface, NRET dominates, which results in relatively weak emission. As the separation distance increases, the LFE effect becomes significant, contributing to the enhancement of intensity. The emission intensity reaches a maximum at an optimal separation distance, in this case about 5 nm. The intensity reduces gradually with further increasing separation distance, accompanied by a gradually reduced weakening electric field. When the separation distance is increased to 25 nm, the emission intensity of PtTFPP enhanced by Ag NPs is comparable to that of bare PtTFPP, which is employed as a baseline reference in this work. At such, far separation distances from the surface of Ag NPs results in insignificant electric field intensity, causing no observable enhancement of dyes from Ag NPs in oxygen sensors. Therefore, the emission enhancement factor of Ag is maximized with 5 nm thickness of SiO_2 in these oxygen sensors. The size diameter of the metal core also affects the emission enhancement. As stated in previous publication [33], the plasmon oscillations can be damped non-radiatively by absorption caused by electron-phonon interactions, and radiatively by the resonant scattering process. The relative contributions from radiative damping through resonant scattering and absorption strongly depend on the particle size [27]. Whereas particles smaller than 30 nm exhibit only absorption,

light extinction of particles larger than 50 nm is dominated by resonant scattering. At 50 nm, both the contribution from scattering and absorption appears to be equal, but their spectra maxima are shifted relative to each other. The spectra peak also red shifts as the NPs' size increase. Considering the scattering and absorption effects, the 95 nm Ag has the strongest emission in the Pt-based oxygen sensors, which agrees well with the results in the previous reports [29, 31].

4. Conclusions

In this work, we prepared core-shell Ag@SiO_2 nanoparticles with different Ag core sizes and shell thicknesses to investigate the intensity enhancement dependence on the NPs' size and metal/dye separation distance in PtTFPP -based oxygen sensors. Our results show that the intensity increases with increasing Ag core size (35-95 nm) and decreases with decreasing shell thickness (5-25 nm). The change in the Ag core size or the shell thickness variation will affect the electric field, which is the key to the overall intensity enhancement of the dyes. Therefore, the change of the Ag core sizes and shell thicknesses will lead to the variation of emission enhancement. Our results promote further insight into the mechanistic understanding of metal-enhanced luminescence in oxygen sensors, which is important to the design and development of noble metal nanoparticles for gas sensors.

Acknowledgements

The U.S. Army Research Office under Grant No. W911NF-18-1-0143 overseen by Dr. Matthew Munson financially supported this effort, for which we are grateful. We also acknowledge the support of the UW CoMotion Commercialization Fellowship Program for Wenwen Yin.

Reference

[1] C. S. Chu, T. W. Sung, Y. L. Lo, Enhanced optical oxygen sensing property based on Pt(II) complex and metal-coated silica nanoparticles embedded in sol–gel matrix, Sensors and Actuators B. 185(2013) 287-292. http:// doi.org/10.1016/j.snb.2013.05.011.

[2] S. M. Peak and A. N. Watkins, Addition of Silica-Coated Ag Nanoparticles to Enhance Luminescence Intensity of Pressure-Sensitive Paints, ACS Appl. Nano Mater. 3(2020) 9813−9821. https:// doi.org/10.1021/acsanm.0c01898.

[3] M. Kang, J. J. Kim, Y. J. Oh, S. G. Park and K. H. Jeong, A Deformable Nanoplasmonic Membrane Reveals Universal Correlations Between Plasmon Resonance and Surface Enhanced Raman Scattering, Adv. Mater. 26(2014) 4510-4514. https://doi.org/10.1002/adma.201305950.

[4] A. I. Dragan and C. D. Geddes, Metal-enhanced fluorescence: The role of quantum yield, Q_0, in enhanced fluorescence, Appl. Phys. Lett. 100(2012) 093115. https://doi.org/10.1063/1.3692105.

[5] Y. Zhang, K. Aslan, M. J. R. Previte, S. N. Malyn and C. D. Geddes, Metal-Enhanced Phosphorescence: Interpretation in Terms of Triplet-Coupled Radiating Plasmons, J. Phys. Chem. B. 110(2006) 25108-25114. https://doi.org/ 10.1021/jp065261v.

[6] M. J. R. Previte, K. Aslan, Y. Zhang and C. D. Geddes, Metal-Enhanced Surface Plasmon-Coupled Phosphorescence, J. Phys. Chem. C. 111(2007) 6051-6059. https://doi.org/ 10.1021/jp0674773.

[7] S. Pan and L. J. Rothberg, Enhancement of Platinum Octaethyl Porphyrin Phosphorescence

near Nanotextured Silver Surfaces, J. Am. Chem. Soc. 127(2005) 6087-6094. https://doi.org/ 10.1021/ja043259g.

[8] C. C. Yu, Y. S. Huang, H. Huang, P. J. Su, T. P. Perng, L. J. Chen, Photocatalytic enhancement of hydrogen production in water splitting under simulated solar light by band gap engineering and localized surface plasmon resonance of $Zn_xCd_{1-x}S$ nanowires decorated by Au nanoparticles, Nano Energy, 67(2020) 104225. https://doi.org/10.1016/j.nanoen.2019.104225.

[9] R. Jiang, B. Li, C. Fang, J. Wang, Metal/Semiconductor Hybrid Nanostructures for Plasmon-Enhanced Applications, Adv. Mater. 26(2014) 5274-5309. https://doi.org/10.1002/adma.201400203.

[10] C. G. Silva, R. Juarez, T. Marino, R. Molinari, H. Garcia, Influence of Excitation Wavelength (UV or Visible Light) on the Photocatalytic Activity of Tatiana Containing Gold Nanoparticles for the Generation of Hydrogen or Oxygen from Water, J. Am. Chem. Soc. 133(2011) 595-602. https://doi.org/ 10.1021/ja1086358.

[11] Y. Ke, X. Wen, D. Zhao, R. Che, Q. Xiong and Y. Long, Controllable Fabrication of Two-Dimensional Patterned VO_2 Nanoparticle, Nanodome, and Nanonet Arrays with Tunable Temperature-Dependent Localized Surface Plasmon Resonance, ACS Nano, 11(2017) 7542–7551. https://doi.org/10.1021/acsnano.7b02232.

[12] X. Li, J. Qian, L. Jiang & S. He, Fluorescence quenching of quantum dots by gold nanorods and its application to DNA detection, Appl. Phys. Lett. 94(2009) 063111. https://doi.org/10.1063/1.3080662.

[13] L. Wang, Q. Song, Q. Liu, D. He and J. Ouyang, Plasmon-Enhanced Fluorescence-Based Core–Shell Gold Nanorods as a Near-IR Fluorescent Turn-On Sensor for the Highly Sensitive Detection of Pyrophosphate in Aqueous Solution, Adv. Funct. Mater. 25(2015) 7017–7027. https://doi.org/10.1002/adfm.201503326.

[14] N. S. Abadeer, M. R. Brennan, W. L. Wilson and C. J. Murphy, Distance and Plasmon Wavelength Dependent Fluorescence of Molecules Bound to Silica-Coated Gold Nanorods, ACS nano. 8(2014) 8392-8406. https://doi.org/ 10.1021/nn502887j.

[15] H. Cang, A. Labno, C. Lu, X. Yin, M. Liu, C. Gladden, Y. Liu & X. Zhang, Probing the electromagnetic field of a 15-nanometre hotspot by single molecule imaging, Nature, 469(2011) 385-388. https://doi.org/10.1038/nature09698.

[16] S. Khatua, P. Paulo, H. Yan, A. Gupta, P. Zijlstra, M. Orrit, Resonant Plasmonic Enhancement of Single-Molecule Fluorescence by Individual Gold Nanorods, ACS nano, 8(2014) 4440-4449. https://doi.org/ 10.1021/nn406434y.

[17] T. Ribeiro, C. Baleizao & J. P. S. Farinha, Artefact-free Evaluation of Metal Enhanced Fluorescence in Silica Coated Gold Nanoparticles, Scientific Reports, 7(2017) 2440. https://doi.org/ 10.1038/s41598-017-02678-0.

[18] F. Tam, G. P. Goodrich, B. R. Johnson and N. J. Halas, Plasmonic Enhancement of Molecular Fluorescence, Nano Lett. 7(2007) 496–501. https://doi.org/10.1021/nl062901x.

[19] J. F. Li, Y. Huang, Y. Ding, Z. Yang, S. Li, X. Zhou, F. Fan, W. Zhang, Z. Zhou, D. Wu, B. Ren, Z. L. Wang and Z. Q. Tian, Shell-isolated nanoparticle-enhanced Raman spectroscopy, Nature, 464(2010) 392–395. https://doi.org/10.1038/nature08907.

[20] X. Zhou, N. M. Andoy, G. Liu, E. Choudhary, K. S. Han, H. Shen and P. Chen, Quantitative super-resolution imaging uncovers reactivity patterns on single nanocatalysts, Nat.

Nanotechnol. 7(2012) 237–241. https://doi.org/10.1038/nnano.2012.18.

[21] J. Yang, F. Zhang, Y. Chen, S. Qian, P. Hu, W. Li, Y. Deng, Y. Fang, L. Han, M. Luqman and D. Zhao, Core-shell Ag@SiO_2@$mSiO_2$ mesoporous nanocarriers for metal-enhanced fluorescence, Chem. Commun. 47(2011) 11618-11620. https://doi.org/10.1039/C1CC15304H.

[22] J. J. Funke and H. Dietz, Placing molecules with Bohr radius resolution using DNA origami, Nat. Nanotechnol. 11(2015) 47–52. https://doi.org/10.1038/nnano.2015.240.

[23] G. P. Acuna, F. M. Moller, P. Holzmeister, S. Beater, B. Lalkens and P. Tinnefeld, Fluorescence Enhancement at Docking Sites of DNA-Directed Self-Assembled Nanoantennas, Science, 338(2012) 506-510. https://doi.org/10.1126/science.1228638

[24] A. L. Feng, M. L. You, L. Tian, S. Singamaneni, M. Liu, Z. Duan, T. J. Lu, F. Xu& M. Lin, Distance-Dependent Plasmon-Enhanced Fluorescence of Upconversion Nanoparticles using Polyelectrolyte Multilayers as Tunable Spacers, Scientific Reports, 5(2015)7779. https://doi.org/10.1038/srep07779.

[25] N. Gandra, C. Portz, L. M. Tian, R. Tang, B. G. Xu, S. Achilefu, S. Singamaneni, Probing Distance-Dependent Plasmon-Enhanced Near-Infrared Fluorescence Using Polyelectrolyte Multilayers as Dielectric Spacers, Angew. Chem. Int. Ed. 53(2014) 866-870. https://doi.org/10.1002/anie.201308516.

[26] A. Guerrero-Martinez, J. Perez-Juste, L.M. Liz-Marzan, Recent Progress on Silica Coating of Nanoparticles and Related Nanomaterials, Adv. Mater. 22(2010) 1182-1195. https://doi.org/10.1002/adma.200901263.

[27] Y. Yan, L. Meng, W. Zhang, Y. Zheng, S. Wang, B. Ren, Z. Yang and X. Yan, High-Throughput Single-Particle Analysis of Metal-Enhanced Fluorescence in Free Solution Using Ag@SiO2 Core–Shell Nanoparticles, ACS Sens. 2(2017) 1369−1376. http://dx.doi.org/10.1021/acssensors.7b00522.

[28] X. Liu, Y. Yin and C. Gao, Size-Tailored Synthesis of Silver Quasi-Nanospheres by Kinetically Controlled Seeded Growth, Langmuir, 29(2013)10559-10565. http://dx.doi.org/10.1021/la402147f.

[29] C. Gao, Y. Hu, M. Wang, M. Chi and Y. Yin, Fully Alloyed Ag/Au Nanospheres: Combining the Plasmonic Property of Ag with the Stability of Au, J. Am. Chem. Soc. 136(2014)7474-7479. http://dx.doi.org/10.1021/ja502890c.

[30] W. Stöber, A. Fink, E. Bohn, Controlled growth of monodisperse silica spheres in the micron size range, J. Colloid Interface Sci. 26(1968) 62−69. https://doi.org/10.1016/0021-9797(68)90272-5.

[31] P. Anger, P. Bharadwaj, L. Novotny, Enhancement and Quenching of Single-Molecule Fluorescence, Phys. Rev. Lett. 96(2006) 113002. https://doi.org/10.1103/PhysRevLett.96.113002.

[32] J. Sun, Z. Li, Y. Sun, L. Zhong, J. Huang, J. Zhang, Z. Liang, J. Chen and L. Jiang, Uniform and reproducible plasmon-enhanced fluorescence substrate based on PMMA-coated, large-area Au@Ag nanorod arrays, Nano Res. 11(2018) 953-965. https://doi.org/10.1007/s12274-017-1708-y.

[33] S. T. Kochuveedu and D.H. Kim, Surface plasmon resonance mediated photoluminescence properties of nanostructured multicomponent fluorophore systems, nanoscale, 6(2014) 4966-4984. https://doi.org/10.1039/C4NR00241E.

Graphical statement:

In the MEL-based oxygen sensors, the emission intensity can be greatly enhanced. The enhanced factor is highly dependent on the separation between the dyes and the noble metal surface and the spectral overlap between the LSPR of noble metal and the excitation spectra of dyes. In this paper, we elaborate on the dependence of the sensitivity and emission intensity on the separation distance from the metal surface by varying the silica shell thickness (5-25 nm), and the Ag NP size (35 nm, 58 nm and 95 nm) in the optical oxygen sensors under varied oxygen pressure. Our results demonstrate that the intensity increases with increasing core size and decreasing shell thickness. The intensity of the 95 nm Ag@5 nm SiO2-PtTFPP based oxygen sensors is the highest among these samples, resulting in 4-9 fold brighter intensity than that of PtTFPP-based oxygen sensors at 0-21% O2.

Nanoparticle core size and spacer coating thickness dependence on metal-enhanced luminescence in optical oxygen sensors

Wenwen Yin[a#], Jiajie Sui[b$], Guozhong Cao[b], Dana Dabiri[a*]

[a] Department of Aeronautics & Astronautics, University of Washington, Seattle WA 98195-2120, USA.

[b] Department of Materials and Engineering, University of Washington, Seattle WA 98195-2120, USA.

Present Addresses:

[#] Sun Yat-sen University, 2 Daxue road, Zhuhai, China, 519000

[$] University of Wisconsin-Madision, 1500 Engineering Drive, Madison, WI 53715

Corresponding Author

*E-mail: dabiri@uw.edu

Novelty statement:

In this work, we prepared core-shell Ag@SiO2 nanoparticles with different Ag core sizes and shell thicknesses to investigate the intensity enhancement dependence on the NPs' size and metal/dye separation distance in PtTFPP-based oxygen sensors. Our results show that the intensity increases with increasing Ag core size (35-95 nm) and decreases with decreasing shell thickness (5-25 nm). The change in the Ag core size or the shell thickness variation will affect the electric field, which is the key to the overall intensity enhancement of the dyes. Therefore, the change of the Ag core sizes and shell thicknesses will lead to the variation of emission enhancement. Our results promote further insight into the mechanistic understanding of metal-enhanced luminescence in oxygen sensors, which is important to the design and development of noble metal nanoparticles for gas sensors.

Highlights:

- We elaborate on the dependence of the sensitivity and emission intensity on the separation distance from the metal surface by varying the silica shell thickness (5-25 nm), and the Ag NP size (35 nm, 58 nm and 95 nm) in the optical oxygen sensors under varied oxygen pressure.
- The intensity increases with increasing core size and decreasing shell thickness. The intensity of the 95 nm Ag@5 nm SiO2-PtTFPP based oxygen sensors is the highest among these samples, resulting in 4-9 fold brighter intensity than that of PtTFPP-based oxygen sensors at 0-21% O_2.
- The Ag@SiO_2 exhibits brighter emission, throughout the range of the oxygen concentration.

Declaration of interests

☑The authors declare that they have no known competing financial interests or personal relationships that could have appeared to influence the work reported in this paper.

☐The authors declare the following financial interests/personal relationships which may be considered as potential competing interests: